Title

Estimating the reaction parameters of oil shale pyrolysis and oil shale grade using temperature transient analysis and inverse modeling

Authors

Lee, Kyung Jae
Finsterle, Stefan
Moridis, George J

Publication Date

2018-06-01

DOI

10.1016/j.petrol.2018.03.020

Peer reviewed

Estimating the reaction parameters of oil shale pyrolysis and oil shale grade using temperature transient analysis and inverse modeling

Kyung Jae Lee[a] Stefan Finsterle[b] George J. Moridis[ac]

Abstract

Grade of oil shale and reaction parameters of in-situ pyrolysismust be identified for the prediction of productivity before actual heating and production. Identification of oil shale grade and reaction parameters depends on laboratory experimentson core samples. However, laboratory-determined parameters can be different from those representing in-situ reservoir conditions. In this study, we use inverse modeling to determine oil shale grade and reaction parameters. The inversions are based on a forward model that simulates heat injection into a well. Temperature at the heating well is affected by a thermal skin effect as a result of a decrease of composite thermal conductivity around the heater due to the decomposition-induced porosity increase. Synthetic observations of heater temperature are generated from a forward simulation. Temperature difference and its derivative are used in synthetic inversions to estimate oil shale grade and parameters of active decomposition reactions with an error below 1%. The proposed methodology of inverse modeling is expected to successfully estimate the oil shale grade and reaction parameters without core sampling and subsequent surface experiments.

Keywords: Reaction parameters, Oil shale grade, Pyrolysis, Temperature transient analysis, Thermal skin effect, Inverse modeling

1. Introduction

Hydrocarbon production from oil shale significantly depends on the grade of oil shale and the parameters of decomposition reactions. Oil shale grade and reaction parameters are typically determined by laboratory experiments on core samples (Burnham and McConaghy, 2014; Campbell et al., 1978; Kar and Hascakir, 2017; Reynolds et al., 1991; Wen and Kobylinski, 1983). However, parameters estimated in the laboratory on the scale of a core sample tend to be conceptually and numerically different from those needed to represent the large-scale behavior under in-situ conditions. In this study, we develop an inversion methodology to estimate the oil shale grade and reaction parameters under in-situ reservoir conditions.

We propose an inverse modeling approach, which examines the use of temperature transient data and the concept of a thermal skin to estimate oil shale grade and decomposition parameters. Similar to pressure transient analyses, temperature transient analyses have been used in oil and gas reservoir engineering to determine productivity, transport properties, and the vertical formation structure (Bahrami and Siavoshi, 2007; Muradov and Davies, 2012; Onur and Cinar, 2017; Sui et al., 2012). In

this study, we observe heater temperature as a system response during in-situ pyrolysis of oil shale in a kerogen-bearing system. We analyze the temperature of an electrical heater operated at a constant heat output rate, while the previous studies analyzed the well temperature during injection or production of fluids.

In combination with the temperature transient analysis, we introduce the concept of a thermal skin effect. Positive hydraulic skin effects in a drawdown test lead to an additional pressure drop at the wellbore, which is induced by decreased permeability around the wellbore due to the mud filtration; and negative hydraulic skin effects lead to a reduced pressure drop at the wellbore, which is induced by increased permeability around the wellbore by stimulation (Lee, 1982). The proposed concept of a thermal skin implies an additional temperature increase at a heater, which is induced by the formation's decreased composite thermal conductivity due to the porosityincrease following oil shale decomposition. The corresponding thermal skin factor thus contains information about decomposition reactivity, which is a function of oil shale grade and reaction parameters.

The objective of this study is to estimate oil shale grade and reaction parameters by inverting transient heater temperature data, as they are effected by the thermal skin. Temperature difference and its derivative are directly computed from the observed heater temperatures. Synthetic data are generated by numerical simulations of heating and in-situ pyrolysis of oil shale, because of the absence of actual field or experimental data. These synthetic data are then used in notional inversions to examine efficacy and accuracy of the proposed method for different thermal conductivities.

2. Mathematical and chemical models

The energy balance equation involving heat accumulation and heat transfer by conduction, convection, and reaction is described as follows (Maes et al., 2016):

$$(1)\partial\partial t[(1-\phi)\rho RCp,RT+\phi\sum\beta\rho\beta S\beta Cp,\beta T]=\nabla\cdot(K\nabla T)-\nabla\cdot(h\beta F\beta)+\sum j\Delta hjrj$$

In the heat accumulation terms on the left-hand side, ϕ is the medium porosity; T [K] is the system temperature; ρR [$kg\cdot m^{-3}$] is the rock grain density; and Cp,R [$J\cdot(kg\cdot K)^{-1}$] is the rock grain specific heat capacity. $S\beta$ is the saturation; and Cp,β [$J\cdot(kg\cdot K)^{-1}$] is the specific heat capacity of phase β. We consider the same temperature of fluid phases and a rock grain in each element, regarding that the time for a rock grain to absorb the heat of fluids is about 10^{-7} s, which means that all fluid phases are at same temperature as a rock grain in a same discrete element (Phillips, 1991; Woods, 1999; Youtsos et al., 2013). In the heat flux terms on the right-hand side, K[$W\cdot(m\cdot K)^{-1}$] is the composite thermal conductivity of the formation; $h\beta$ [$J\cdot kg^{-1}$] is the specific enthalpy of phase β; and $F\beta$ [$kg\cdot m^{-2}\cdot s^{-1}$] is the flow rate of phase β, which is described by Darcy equation. In the reactive heat term on the right-hand side, Δhj [$J\cdot kg^{-1}$] is the reaction

enthalpy; and rj [kg·m^{-3}·s^{-1}] is the reaction rate of *j*-th reaction. The detailed equations for Cp,β, Fβ, and hβcan be found in Lee et al. (2016).

The most active decomposition reactions of oil shale pyrolysisare summarized in Table 1 (Braun and Burnham, 1992; Youtsos et al., 2013). When kerogen in a porous medium is heated to a high temperature, it decomposes into fluid and solid components. Heavy oil and coke 1, which are generated from the kerogen decomposition, also decompose into secondary products. The reaction rate of each reaction is determined by using the Arrhenius law of first order as follows:

(2)rj=Ajexp(−EjRT)Cj=KjCj

where, Cj [kg·m^{-3}] is the concentration of reactant *j*; Aj [s^{-1}] is the frequency factor; Ej [kJ·mol^{-1}] is the activation energy; Kj [s^{-1}] is the reaction rate constant; and R (= 8.314·10^{-3}) [kJ·mol^{-1}·K^{-1}] is the gas constant.

Table 1. Most active decomposition reactions of oil shale pyrolysis(Braun and Burnham, 1992; Youtsos et al., 2013).

Reactions	Frequency factor [s^{-1}]	Activation energy [kJ·mole^{-1}]	Reaction enthalpy [kJ·mole^{-1}]	Magnitude of reaction rate constant [a] [s^{-1}]
Kerogen → 0.279 Heavy oil + 0.143 Light oil + 0.018 Hydrocarbon gas + 0.005 Methane + 0.555 Coke 1	3.0 × 10^{13}	213.384	−335	10^{-8}-10^{-5}
Heavy oil → 0.373 Light oil + 0.156 Hydrocarbon gas + 0.03 Methane + 0.441 Coke	1.0 × 10^{13}	225.936	−46.5	10^{-10}-10^{-6}

Reactions	Frequency factor [s^{-1}]	Activation energy [kJ·mole^{-1}]	Reaction enthalpy [kJ·mole^{-1}]	Magnitude of reaction rate constant[a] [s^{-1}]
2 Coke 1 → 0.031 Hydrocarbon gas + 0.033 Methane + 0.936 Coke 2	1.0×10^{13}	225.936	−46.5	10^{-10}-10^{-6}

a. Reaction rate constants were computed for temperatures between 250 and 350 °C, where the reactions were active.

Dynamic change of the reservoir porosity, which is defined by the volumetric ratio of void space to the bulk formation, can be computed by accounting for the amount of individual solid components:

(3)$\phi = \phi i + V_{kerogen,i} C_{kerogen,i} (C_{kerogen,i} - C_{kerogen} - C_{cokes})$

where, ϕi is the initial porosity; $V_{kerogen,i}$ is the initial volume fraction of kerogen in the porous media; $C_{kerogen,i}$ [kg·m^{-3}] is the initial concentration of kerogen; and $C_{kerogen}$ [kg·m^{-3}] and C_{cokes} [kg·m^{-3}] are the concentrations of kerogen and cokes, respectively. In Eq. (3), the pore expansion by increasing temperature and the heating-induced pressurization is not included because of its insignificant magnitude. Assuming a pore compressibility of 4.35×10^{-10} Pa^{-1} and a thermal expansivity of 10^{-5} K^{-1}, factors of the pore expansion by the pressurization and increasing temperature are on the order of 10^{-4} and 10^{-3}, respectively. Changes in porosity due to changing temperature and pressure are fully accounted for in our numerical model. In addition to this, dynamically changing permeability, tortuosity, and composite thermal conductivity are accounted in the numerical model, so that we can accurately simulate the flow of heat and fluid with changing porosity. Kozeny-Carman equation and Millington-Quirk equation are used for porosity-dependent permeability and tortuosity, respectively (Krauss and Mays, 2014; Millington and Quirk, 1961). The computation of composite thermal conductivity is covered in section 3.2.

The solid concentrations of kerogen and cokes are described by the following equation:

(4)$\partial C_\kappa / \partial t = \sum j s_\kappa r_j$

where C_κ [$kg \cdot m^{-3}$] is the concentration of component κ; and s_κ is the stoichiometry number of component κ in the *j*-th reaction. From Eqs. (3), (4), it is expected that the decomposition reactions affect the porosity of the system during the heating process.

Regarding the reactions and flux terms, the concentrations of fluid components are described as a following form of differential equation.

$$(5)\partial C_\kappa \partial t = \sum_j s_\kappa r_j - \nabla \cdot (F_\kappa)$$

where, F_κ [$kg \cdot m^{-2} \cdot s^{-1}$] is the flow rate of fluid component κ, which is a sum of convective and diffusive flow rates of component.

Initially, the pores of the system are homogeneously filled with kerogen and small amount of water and gas phases. Here, the initial conditions of the system are as follows.

$$(6)T(t=0, r \geq 0) = T_i$$

$$(7)C_{kerogen}(t=0, r \geq 0) = C_{kerogen,i}$$

where, T_i [K] is the initial temperature of the system. The boundary conditions of the system are as follows.

$$(8)T(r \to \infty) = T_i$$

$$(9)C_{kerogen}(r \to \infty) = C_{kerogen,i}$$

Fluid production or injection is not implemented during the heating process, and component mass in the whole system is conserved as follows.

$$(10)\sum_j C_j = constant$$

where, j = all components in the system.

3. Problem description

We consider an infinite, isotropic, and homogeneous porous medium, which initially contains kerogen and small amount of water and gas phases, for the mathematical simplification. Here, constant rate of heat is radially transferred from an electrical heating well to the surrounding formation. We will focus on the heating period less than a year, before the convective heat flow gets dominant as the porous medium becomes permeable by severe decomposition of kerogen.

3.1. Equation of temperature

Majority of raw oil shale formations is impermeable, and conductive heat flow is dominant in such systems in the early time period of in-situ conversion. The convective heat flow term on the right hand side of Eq. (1) then can be removed; and the terms of conductive heat flow and reactive heat are left.

Now we check if the reactive heat is significant for temperature change, by applying generally-used properties of rich oi shales. Oil shale grade of 20 gpt (=gal/ton) gives the kerogen amount of 25.02 vol% in oil shale formation

(Eseme et al., 2007). Using the heat capacity of kerogen of 2740 $J\,(kg\,K)^{-1}$(Berkovich et al., 2000), the molecular weight of kerogen of 0.647 $kg\,mol^{-1}$, the density of kerogen of 1200 $kg\,m^{-3}$ (Youtsos et al., 2013), and the oil shale rock density of 2600 $kg\,m^{-3}$, we have the kerogen concentration of 300.2741 $kg\,m^{-3}$(=0.000206 $mol\,kg^{-1}$). Using these values, we expect that the temperature change by the reactions will be 0.0252 K at the most. This is insignificant, considering that the temperature change by the heating will be above 300 K; and we will ignore the reactive heat term. Now Eq. (1) is reduced to the following heat conduction equation.

$$(11)\partial\partial t[(1-\phi)\rho RCp,RT+\phi\sum\beta\rho\beta S\beta Cp,\beta T]=\nabla\cdot(K\nabla T)$$

By assuming the constant density and specific heat capacity of the bulk oil shale rock and applying the equation to a radial coordinate system, we have the following temperature diffusivity equation.

$$(12)1r\partial\partial r[r\partial T\partial r]=\rho CpK\partial T\partial t$$

In order to get the solution of Eq. (12), we mirror the solution approach of flow diffusivity equation (Lee, 1982). By applying a set of dimensionless variables of radius, time, and temperature, as defined in Eq. (13), we have a dimensionless partial differential equation as shown in Eq. (14).

$$(13)rD=rrw,tD=Kt\rho Cprw,TD=2\pi Khqh(T-Ti)$$

$$(14)1rD\partial\partial rD[rD\partial TD\partial rD]=\partial TD\partial tD$$

where, rw [m] is the radius of the wellbore; qh [$J\cdot s^{-1}$] is the injection rate of heat; and h [m] is the heater length, which is identical to the thickness of oil shale formation, respectively. By applying the dimensionless variables, the outer and inner boundary conditions of temperature are described as follows.

$$(15)TD(tD=0,rD\geq 0)=0$$

$$(16)[rD\partial TD\partial rD]rD=1=-1$$

The solution of Eq. (14) with boundary conditions of Eqs. (15), (16) is described as follows (Lee, 1982).

$$(17)TD(tD,rD)=-12Ei(-rD4tD)=12E1(rD4tD)$$

which is a line source solution that is applied in case of tD>10. When we use $K = 2.0\,W\,(m\,K)^{-1}$, $\rho = 2600\,kg\,m^{-3}$,$Cp = 1500\,J\,(kg\,K)^{-1}$, $rw = 0.1\,m$, $h = 10\,m$, and $qh = 8500\,J\,s^{-1}$, the range of applicable time for Eq. (17)becomes t>1.95·105 sec. Even simpler, Eq. (17) can be described by log approximation as follows, when tD>25rD(Lee, 1982).

$$(18)TD(tD,rD)=12\ln(4tDe\gamma rD)$$

where, γ is the Euler's constant (=0.577216 ⋯). The range of applicable time for Eq. (18) is t>4.88·105 sec, at the heating well ($rD = 1$).

To more accurately compute the analytical solution of temperature, we numerically inverted Laplace domain equation of cylindrical solution, which is described as follows (Lee, 1982).

(19)T¯D(rD,μ)=K0(μrD)μμK1(μ)

where, μ is the Laplace domain variable. By using Gaver-Stehest algorithm, the Laplace domain solution in Eq. (19) can be inverted into real domain solution (Stehfest, 1970).

3.2. Thermal skin effect

In the oil shale-bearing system, porosity around the heat injection well dynamically increases as the decomposition reactions proceed. Composite thermal conductivity of the formation, which is described as the following equation, changes along with evolving porosity.

(20)K=KR(1−ϕ)+ϕ∑βSβKβ

where, KR [W·(m·K)$^{-1}$] is the thermal conductivity of dry rock including solid components; and Kβ [W·(m·K)$^{-1}$] is the thermal conductivity of fluid phase β, respectively.

The schematic concept of decomposing zone and non-decomposing zone are shown in Fig. 1. Considering that the thermal conductivities of oil and gas are less than 0.1 W (m K)$^{-1}$ in the reservoir conditions, the composite thermal conductivity of kerogen-decomposing zone around the heat injection well is lower than that of surrounding non-decomposing zone. In this circumstance, the temperature at the heat injection well (heater) is deviated from that of a heater in a formation of uniform thermal conductivity.

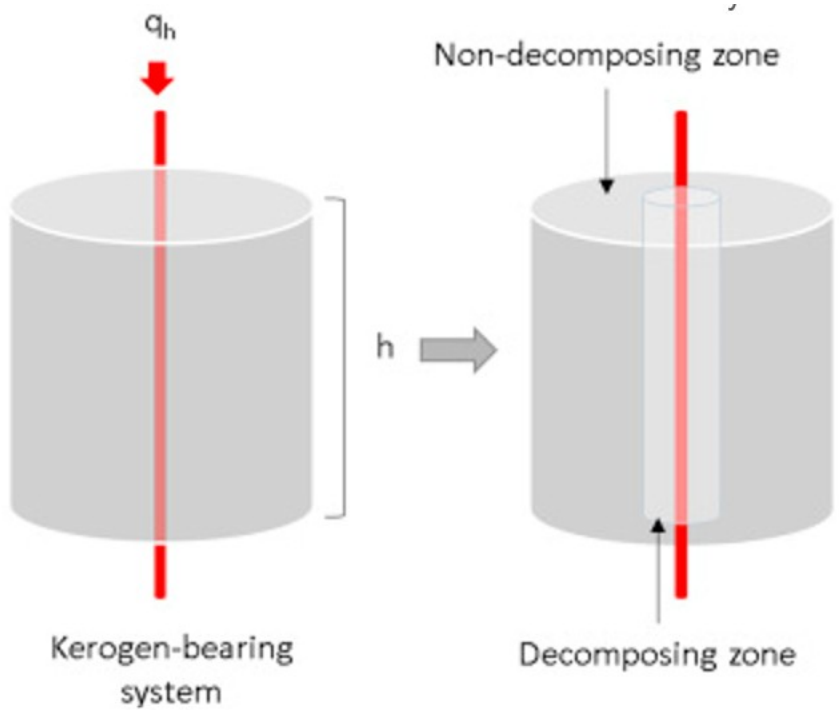

Fig. 1. Schematic concept of decomposing zone near the heater and non-decomposing zone, in the kerogen-bearing system.

We define the thermal skin factor as a difference between dimensionless heater temperature of analytic solution (TwD,analytic) without reactions occurring and the heater temperature in the kerogen-bearing system (TwD,decomp), as follows.

(21)S=TwD,decomp−TwD,analytic

The dimensionless temperature of the heater and thermal skin effect are expected to provide the information of parameters of decomposition reactions, recalling Eqs. (3), (4), (20).

3.3. Temperature transient analysis

We conducted a numerical simulation of heating, by using the input parameters in Table 2. In the simulation, our in-house numerical simulator was used, which has been developed based on the variant of TOUGH+—successor of TOUGH2 family of code (Lee et al., 2016; Moridis et al., 2006; Pruess et al., 1999). The simulator describes the in-situ upgrading of oil shales in non-isothermal and multiphase-multicomponent systems, using a fully-implicit solution approach. We obtained the confidence in the code by matching simulation results with field production data (Fowler and Vinegar, 2009; Lee et al., 2016; Vinegar, 2006).

Table 2. Input parameters of the heating simulation.

Input parameters	Values	Input parameters	Values
ϕi [−] (Initial porosity)	0.015	Pi [MPa] (Initial system pressure)	20.7
Vkerogen,i [−] (Initial kerogen volume fraction)	0.25	Ti [K] (Initial system temperature)	303.15
ρR [$kg \cdot m^{-3}$] (Dry rock density)	2600	rw [m] (Heating well radius)	0.1
Cp,R [$J \cdot (kg \cdot K)^{-1}$] (Dry rock specific heat capacity)	1500	h [m] (Thickness of heating interval)	10
KR [$W \cdot (m \cdot K)^{-1}$] (Dry rock thermal conductivity)	2.0	qh [$J \cdot s^{-1}$] (Heat injection rate)	8500

The heater temperature was observed from 20 days to 360 days, with an observation frequency of 10 days. The temperature difference at the heater well (ΔT) and its derivative (ΔT') were computed as follows.

(22)ΔT=Tw−Tw,i

(23)ΔT'=dΔTdln(t)

where, Tw [°C] is the heater temperature; Tw,i [°C] is the heater initial temperature; ΔT' [°C/ln (sec)] is the ΔTderivative; and t [sec] is time, respectively. The computed ΔTand ΔT' are presented in the log-log plot in Fig. 2 (a). Thermal skin factor as a function of time is presented in Fig. 2 (b). The expanded plots of ΔT and ΔT' in late time period are provided in Fig. 3. Here, the analytical solutions of ΔT and ΔT' were computed by numerical inversion of cylindrical solution in Laplace domain.

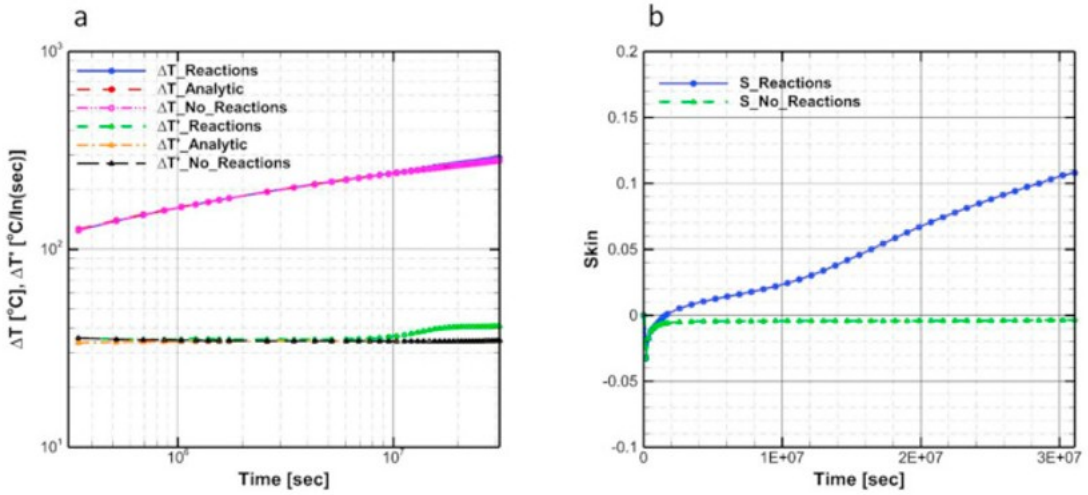

Fig. 2. (A) Log-log plot of ΔT and ΔT', (b) evolution of thermal skin factor, S.

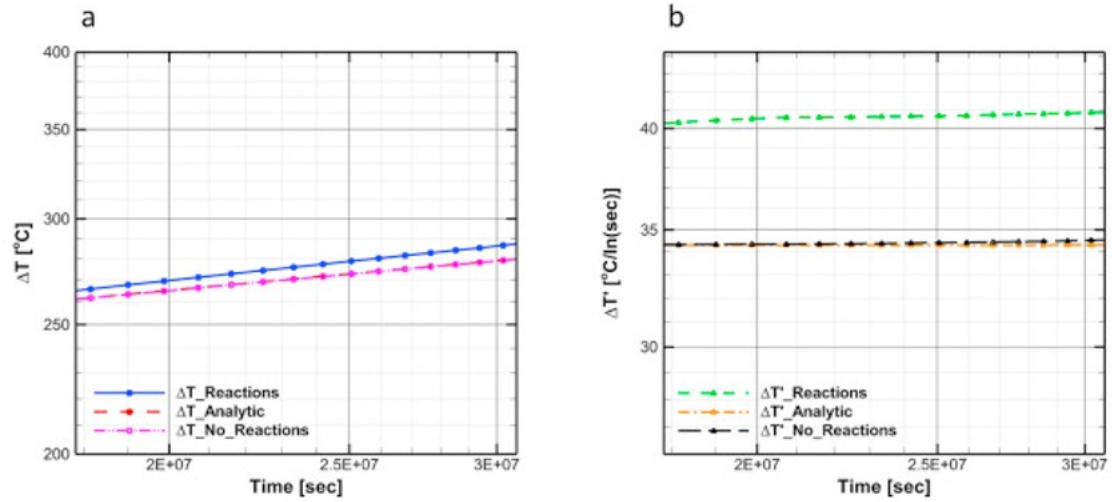

Fig. 3. (A) Log-log plot of ΔTin late time, (b) log-log plot of ΔT' in large time.

From Eqs. (13), (18), we can obtain the following equation for thermal conductivity.

(24)K=qh4πhΔT'

where, ΔT' should be obtained in the infinite-acting radial flowregime in the log-log plot, which is shown as the zero slope-region of ΔT' versus time.

In Fig. 2 (a), the analytic solution and the numerical simulation results of no-reactions-case are also presented; and they show the radial flow regime throughout the heating process. In these cases, we can obtain the composite thermal conductivity of the formation of $1.9715\,\mathrm{W\,(m\,K)^{-1}}$, by using Eq. (24). This shows the agreement with the composite thermal conductivity, which can be obtained with Eq. (20), considering that the thermal conductivity of fluid phases is around $0.10\,\mathrm{W\,(m\,K)^{-1}}$ in the reservoir condition. When decomposition reactions occur, we observe the higher ΔT and ΔT' in the log-log plot by the thermal skin effect. In Fig. 3 (b), we observe that the slightly higher ΔT' in the simulation result of no-reaction case than the analytical solution in late time. This is because, the pores expand by increasing temperature and heating-induced pressurization, and hence decreasing composite thermal conductivity.

The effect of KR on ΔT and ΔT' are presented in Fig. 4. The higher the KR, the lower the ΔT and ΔT' at the heater, owing to more vigorous heat transfer to the surrounding formation. It is also remarkable that ΔT' increases with decreasing slope of ΔT; and this is because, dln(t) decreases more rapidly than dΔT decreases.

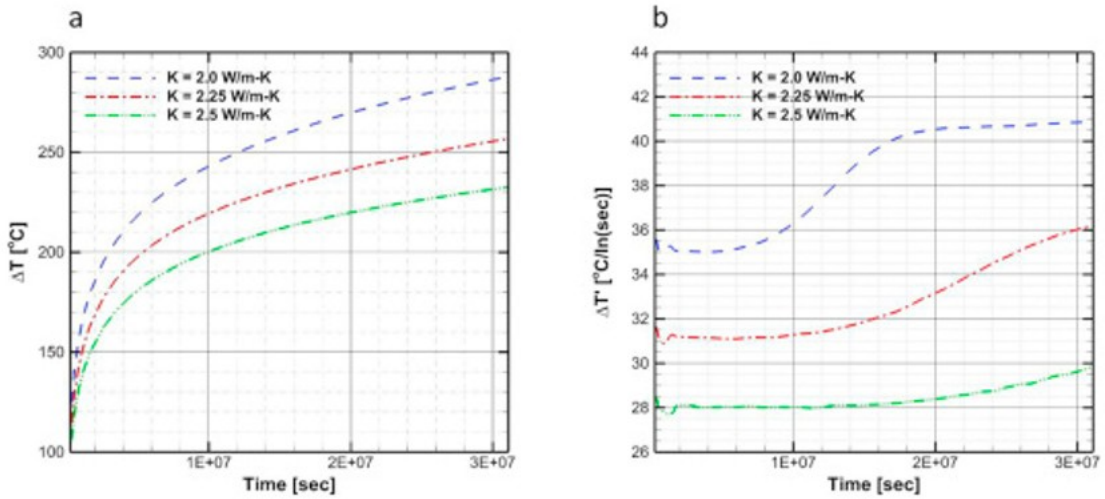

Fig. 4. Effect of thermal conductivity of dry rock. (a) ΔT, (b) ΔT'.

The thermal skin factor caused by the decomposition reactions was compared with that in the case without decomposition reactions. Thermal skin factor caused by the decomposition reactions was continuously increasing during the heating process and approached 0.11 at $\mathrm{t} = 3.11 \times 10^{7}\,\mathrm{s}$ (= 360 days) (Fig. 2 (b)). Thermal skin factor in the case without reactions

showed the negative values in moderate magnitude. This has been caused by the heat convection due to expansion induced fluid flow, which has not been included in the analytic solution. We can understand it as similar phenomena to the negative skin by stimulation and increased permeability in pressure transient testing.

4. Inverse modeling

We conducted an inverse modeling to estimate unknown oil shale grade and reaction parameters by observing heater temperature. Three different cases of thermal conductivities of 2.0, 2.25, and 2.5 $W\,(m\,K)^{-1}$ for dry rock were investigated. Before the inverse modeling, we conducted a local sensitivity analysis to quantify the effect of unknown parameters on the observation data. In the local sensitivity analysis and following inverse modeling, we used the simulation-optimization framework of iTOUGH2 combined with PEST protocol (Finsterle, 1999; Finsterle and Zhang, 2011). It coupled our numerical simulator to the analysis toolkit of iTOUGH2.

4.1. Local sensitivity analysis

We conducted a local sensitivity analysis of ΔTand ΔT' to the oil shale grade and activation energies of three decomposition reactions in Table 1. Note that ΔT and ΔT' imply the information of thermal skin factor and formation thermal conductivity, respectively (see Eqs. (21), (24)). In the local sensitivity analysis, sensitivity coefficients are computed by the following equation.

(25)Sij=∂zi∂pj

where, Sij is the sensitivity coefficients of *i*-th output response, zi, with respect to the *j*-th parameter, pj. We use the concept of scaled sensitivity coefficients, S¯ij, to directly compare the sensitivity to each other by making the sensitivity coefficients dimensionless.

(26)S¯ij=Sij·σpjσzi

where, σpj is the scaling factor of parameter; and σzi is the scaling factor of output response. We used the parameter scaling factors of 2.5 gpt and 4 $kJ\,mol^{-1}$ for the oil shale grade and activation energies. Output scaling factors were 0.5 °C and 0.1 °C/ln (sec) for ΔT and ΔT', respectively. Each scaling factor of parameters and output measurements has been determined by following criteria:

(1) Scaling factor of 2.5 gpt-oil shale grade is obtained by using 3.5 vol%-variation of organic matter content, which is a value in the generally taken range of 3–5%-porosity variation for inversion studies, considering that the organic matter content is directly related to organic porosity (Finsterle, 1999; Smith, 1976).

(2) Scaling factor of 4 $kJ{\cdot}mol^{-1}$-activation energies is chosen to include 90% of sample measurements around the average, as obtained from

the paperpresenting the reaction model of oil shale pyrolysis(Braun and Burnham, 1992).

(3) Scaling factor of 0.5 °C-ΔT is chosen as a measurement error of thermometers (Steingrímsson, 2013).

(4) Scaling factor of 0.1 °C/ln (sec)- ΔT' is chosen, regarding the scaling factor of ΔT and the relative magnitude between ΔT and ΔT' throughout the process.

The results of sensitivity analysis are shown in Fig. 5. The case of $KR = 2.0\,W\,(m\,K)^{-1}$ shows the most sensitive ΔT and ΔT' to the unknown parameters among the cases. This is because, more concentrated heat around the heater in the case of $KR = 2.0\,W\,(m\,K)^{-1}$ than the cases of higher KRcaused more active decomposition reactions, which were the function of input (unknown) parameters, and hence more strongly affected output data of ΔT and ΔT' . ΔT' was more sensitive than ΔT to the unknown parameters, and the effects of activation energies of heavy oil and coke 1 decomposition reactions were not ignorable in the case of $KR = 2.0\,W\,(m\,K)^{-1}$, while the effects were insignificant in the cases of $KR = 2.25$ and $2.5\,W\,(m\,K)^{-1}$.

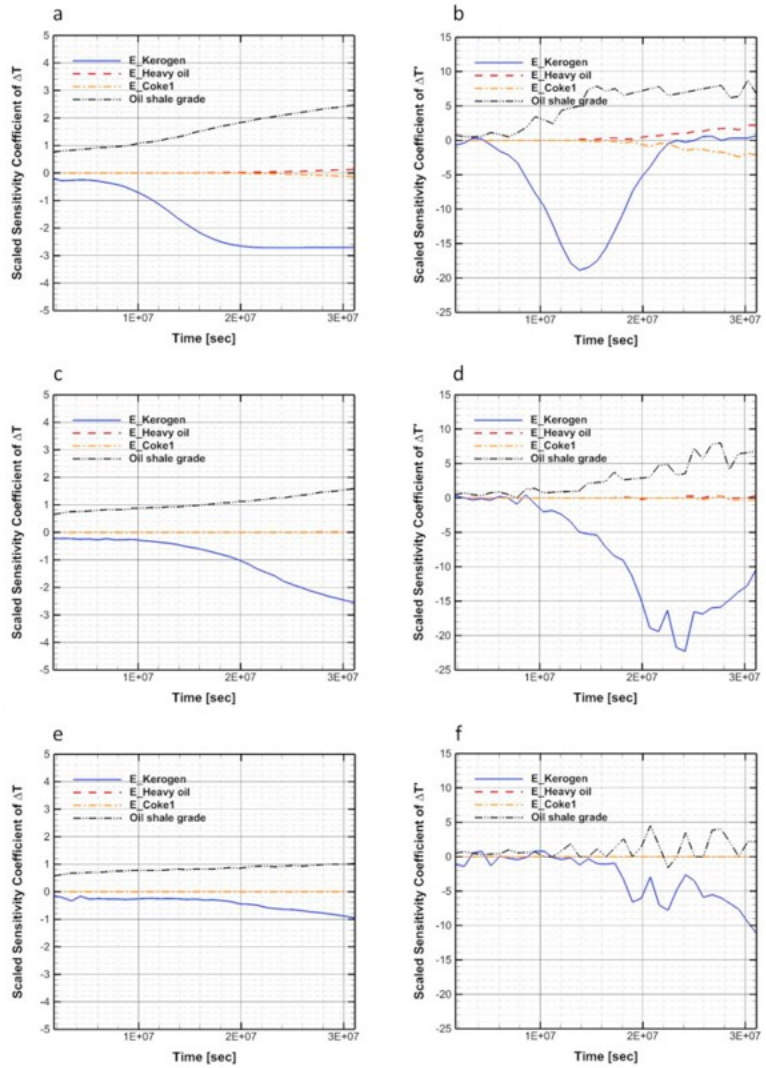

Fig. 5. Scaled sensitivity coefficients of output responses as a function of time, with respect to the oil shale grade and activation energies of decomposition reactions of kerogen, heavy oil, and coke 1.

(a) $\Delta T(KR = 2.0\,W\,(m\,K)^{-1})$, (b) $\Delta T'$ $(KR = 2.0\,W\,(m\,K)^{-1})$,
(c) $\Delta T(KR = 2.25\,W\,(m\,K)^{-1})$, (d) $\Delta T'$ $(KR = 2.25\,W\,(m\,K)^{-1})$,
(e) $\Delta T(KR = 2.5\,W\,(m\,K)^{-1})$, (f) $\Delta T'$ $(KR = 2.5\,W\,(m\,K)^{-1})$

4.2. Parameter estimation by inverse modeling

4.2.1. Input parameters of various cases

The oil shale grade and parameters of decomposition reactions were estimated in various cases. Table 3 contains the parameters of true models, which were used in the generation of synthetic data. Three true models of $KR = 2.0$, 2.25, and $2.5\,W\,(m\,K)^{-1}$ are indicated.

Table 3. Parameters of the true models.

	KR **[W·(m·K)$^{-1}$]**	M **[gpt]**	Ekerogen **[kJ·mole^{-1}]**	EHeavyoil **[kJ·mole^{-1}]**	ECoke1 **[kJ·mole^{-1}]**
True models	2.0 (case 1, 4, 5), 2.25 (case 2), 2.5 (case 3)	20	213.38	225.94	225.94

Table 4 shows the details of inverse modeling for case 1 (KR= 2.0 $W\,(m\,K)^{-1}$), case 2 (KR= 2.25 $W\,(m\,K)^{-1}$), and case 3 (KR= 2.5 $W\,(m\,K)^{-1}$). In the cases 1, 2, and 3, the unknown parameters of oil shale grade (M) and the activation energy of kerogen decomposition (Ekerogen) were estimated based on the observation of ΔT. ΔT was observed starting from 20 days with a measurement frequency of 10 days. The end of observation times of 120 days, 240 days, and 360 days were set in each case to analyze the accuracy of inverse modeling as a function of observation time.

Table 4. Cases 1, 2, and 3 to analyze the impact of KR and data observation time. ΔT was observed with a frequency of 10 days, in every case. Note that oil shale grade (M) and activation energy of kerogen decomposition (Ekerogen) were unknown, and their initial guesses of 25 gpt and 217.38 $kJ\,mol^{-1}$ were used for the inverse modeling, respectively. Also note that EHeavyoil and ECoke1 are known and fixed as true values.

	KR **[W·(m·K)$^{-1}$]**	**Observation time [days]**
True model	2.0, 2.25, 2.5	
Case 1-1	2.0	20–360
Case 1–2	2.0	20–240
Case 1–3	2.0	20–120
Case 2-1	2.25	20–360
Case 2-2	2.25	20–240
Case 2–3	2.25	20–120
Case 3-1	2.5	20–360
Case 3-2	2.5	20–240
Case 3-3	2.5	20–120

In case 4 and case 5, we additionally analyzed the activation energies of heavy oil (EHeavyoil) and coke 1 (ECoke1) decompositions. Case 4 and case 5 were conducted in the formation with KR $= 2.0\,W\,(m\,K)^{-1}$. (Recall that the effects of heavy oil and coke 1 decompositions were only detectable by the observed ΔT and ΔT' in the case of KR $= 2.0\,W\,(m\,K)^{-1}$, from the previous sensitivity analysis.)

In case 4, we analyzed the effect of incorrect EHeavyoil and ECoke1 on the inverse modeling. Table 5 shows the parameters of case 4. In this case

4, ΔT was observed starting from 20 days to 360 days with a measurement frequency of 10 days.

Table 5. Case 4 to analyze the impact of incorrect parameters. ΔTwas observed from 20 to 360 days with a frequency of 10 days, in every case. Note that KR $= 2.0\,\mathrm{W\,(m\,K)^{-1}}$; M and Ekerogen were unknown, and their initial guesses of 25 gpt and 217.38 $\mathrm{kJ\,mol^{-1}}$were used for the inverse modeling, respectively.

	EHeavyoil **[kJ·mole^{-1}] (fixed)**	ECoke1 **[kJ·mole^{-1}] (fixed)**
Case 4-1	229.94 (incorrect value)	225.94 (true value)
Case 4-2	225.94 (true value)	229.94 (incorrect value)

In case 5, we conducted a two-step inversion. Table 6 shows the implementation details of case 5. In the first step from 20 days to 240 days, ΔT was observed with a measurement frequency of 10 days to estimate M and Ekerogen. In the first step of inverse modeling, EHeavyoil and ECoke1 were assumed at 221.94 $\mathrm{kJ\,mol^{-1}}$ and 229.94 $\mathrm{kJ\,mol^{-1}}$, respectively. In the second step from 250 days to 360 days, ΔT' was observed with a measurement frequency of 10 days to estimate EHeavyoil and ECoke1. Here, M and Ekerogen, which were obtained with the first step of inverse modeling, were assumed.

Table 6. Case 5 of two-step inversion. Note that KR $= 2.0\,\mathrm{W\,(m\,K)^{-1}}$; M, Ekerogen, EHeavyoil, and ECoke1 were unknown. Inverse modeling for M and Ekerogen was conducted by observing ΔT from 20 to 240 days with a measurement frequency of 10 days; and inverse modeling for EHeavyoil and ECoke1 was conducted by observing ΔT'from 250 to 360 days with a measurement frequency of 10 days.

	Observation data	**Observation time [days]**	M **[gpt]**	Ekerogen**[kJ·mole^{-1}]**	EHeavyoil**[kJ·mole^{-1}]**	ECoke1**[kJ·mole^{-1}]**
Case 5-first step	ΔT	20–240	25	217.38	221.9 (fixed)	229.94 (fixed)
Case	ΔT'	250–	obtained	obtained from the	221.94	229.94

	Observation data	Observation time [days]	M [gpt]	Ekerogen[kJ·mole^{-1}]	EHeavyoil[kJ·mole^{-1}]	ECoke1[kJ·mole^{-1}]
5-second step		360	from the first step	first step		

4.2.2. Results of inverse modeling

Results of the inverse modeling are provided in Table 7. In the inverse modeling, objective functions were computed based on a least-square method. In overall, the inversion performance was excellent, with the maximum relative errors of 3.93% and 1.43% for the estimation of M and Ekerogen, respectively; case 1 of KR $= 2.0\,\mathrm{W\,(m\,K)^{-1}}$ showed the best performance of inverse modeling with the lowest standard deviations of estimated parameters. This is because, the ΔTand ΔT' were more sensitive to the unknown parameters in the case of KR $= 2.0\,\mathrm{W\,(m\,K)^{-1}}$ than KR $= 2.25\,\mathrm{W\,(m\,K)^{-1}}$and KR $= 2.5\,\mathrm{W\,(m\,K)^{-1}}$, which means that the measurement data more strongly imply the effect of unknown parameters. The minimum observation time can be determined based on KR and maximum allowable uncertainty of parameter prediction, because the inversion performance is a function of KR and observation time.

Table 7. Results of inverse modeling. The numbers in the parentheses are the standard deviations of estimated parameters.

True model	M **[gpt]**	Ekerogen**[kJ·mole^{-1}]**	EHeavyoil**[kJ·mole^{-1}]**	ECoke1**[kJ·mole^{-1}]**
	20.000	**213.380**	**225.940**	**225.940**
Case 1-1	20.000 (±1.097)	213.381 (±1.441)	–	–
Case 1-2	20.000 (±1.	213.380 (±1.517)	–	–

True model	M **[gpt]**	Ekerogen**[kJ·mole⁻¹]**	EHeavyoil**[kJ·mole⁻¹]**	ECoke1**[kJ·mole⁻¹]**
	20.000	**213.380**	**225.940**	**225.940**
	150)			
Case 1-3	19.999 (±2.680)	213.377 (±9.270)	–	–
Case 2-1	20.181 (±0.930)	213.552 (±1.357)	–	–
Case 2-2	20.315 (±1.485)	213.805 (±4.166)	–	–
Case 2-3	20.460 (±9.119)	214.651 (±44.506)	–	–
Case 3-1	20.146 (±1.540)	213.591 (±4.981)	–	–
Case 3-2	20.773 (±5.341)	216.440 (±23.616)	–	–
Case 3-3	20.786 (±6.737)	216.276 (±30.744)	–	–
Case 4-1	19.968 (±1.	213.401 (±1.434)	–	–

True model	M **[gpt]**	Ekerogen**[kJ·mole^{-1}]**	EHeavyoil**[kJ·mole^{-1}]**	ECoke1**[kJ·mole^{-1}]**
	20.000	**213.380**	**225.940**	**225.940**
	088)			
Case 4-2	20.299 (±0.918)	213.652 (±0.983)	–	–
Case 5	19.976 (±1.160)	213.313 (±1.529)	225.778 (±4.232)	226.754 (±5.886)

Case 4 showed that the effect of incorrect EHeavyoil and ECoke1 was ignorable in the inversion of M and Ekerogen. Much lower scaled sensitivity coefficients of ΔT and ΔT' to EHeavyoil and ECoke1 than those of M and Ekerogen underpin the result (Fig. 5). In case 5, the estimated parameters of EHeavyoil and ECoke1 showed higher uncertainty than M and Ekerogen. However, the inversion performance of EHeavyoil and ECoke1by the two-step is good, regarding that their relative errors were around 0.08% and 0.35%.

Fig. 6 and Fig. 7 show the match of thermal skin factor in each case. Here, we presented the thermal skin factor rather than actual observation data of ΔT, because the discrepancy between the true model and calibrated model is more easily visualized using thermal skin factor. (Recall thermal skin factor is proportional to ΔT.) In Fig. 6, it is shown that there are tiny discrepancies in thermal skin factor between the true model and the calibrated models in case 2 and case 3 at late time period, when observation time = 120 days. This is because, ΔT and ΔT' started to actively respond to the unknown parameters after 120 days in the case 2 and case 3, as shown in Fig. 5. Fig. 7 (a) shows that the incorrect EHeavyoil and ECoke1 made slight discrepancy between the true model and the calibrated model at the late time period of $t > 2.8 \times 10^7$ s, while Fig. 7 (b) of two-step inversion shows more accurate match even in the late time period.

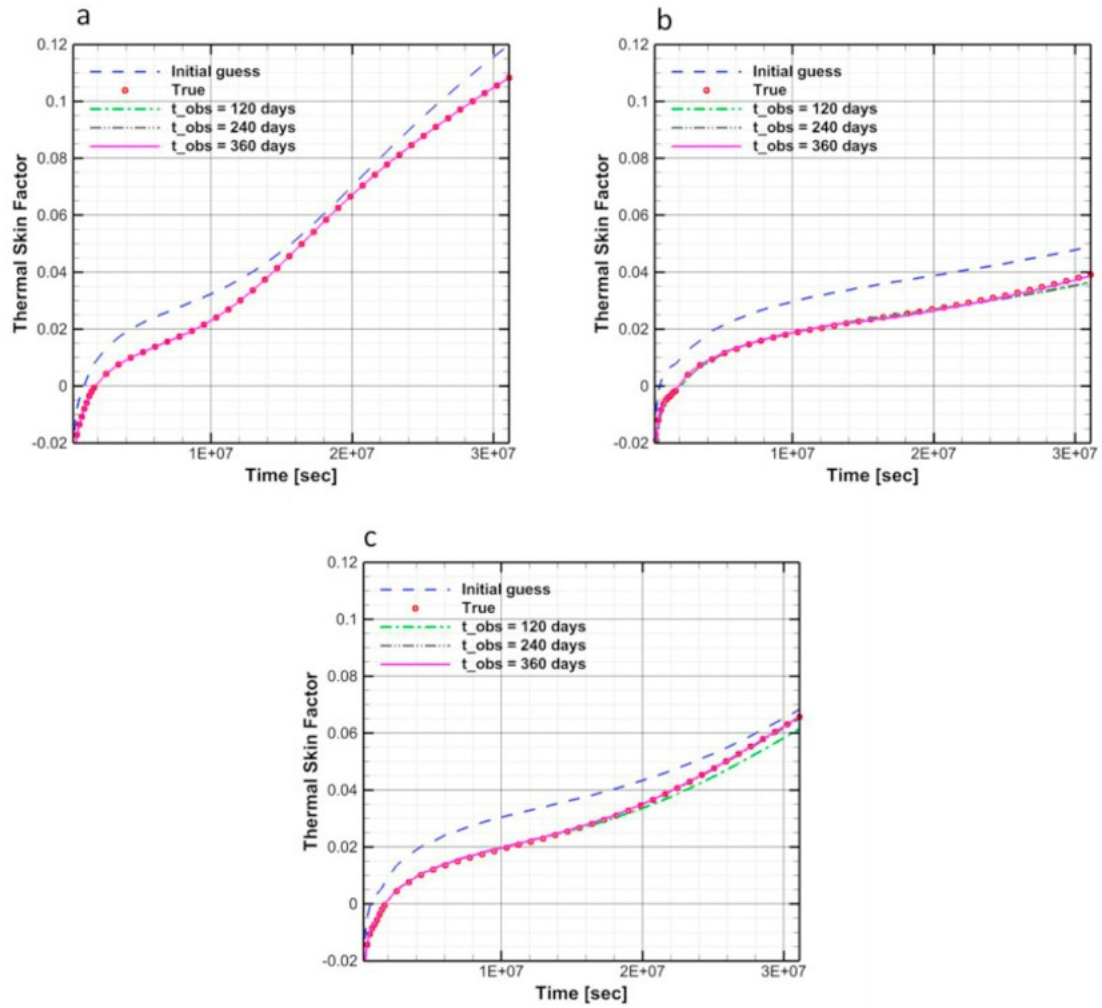

Fig. 6. Match of thermal skin factor as a function of time. (a) Case 1 (KR $= 2.0\,\mathrm{W\,(m\,K)^{-1}}$), (b) case 2 (KR $= 2.25\,\mathrm{W\,(m\,K)^{-1}}$), (c) case 3 (KR $= 2.5\,\mathrm{W\,(m\,K)^{-1}}$).

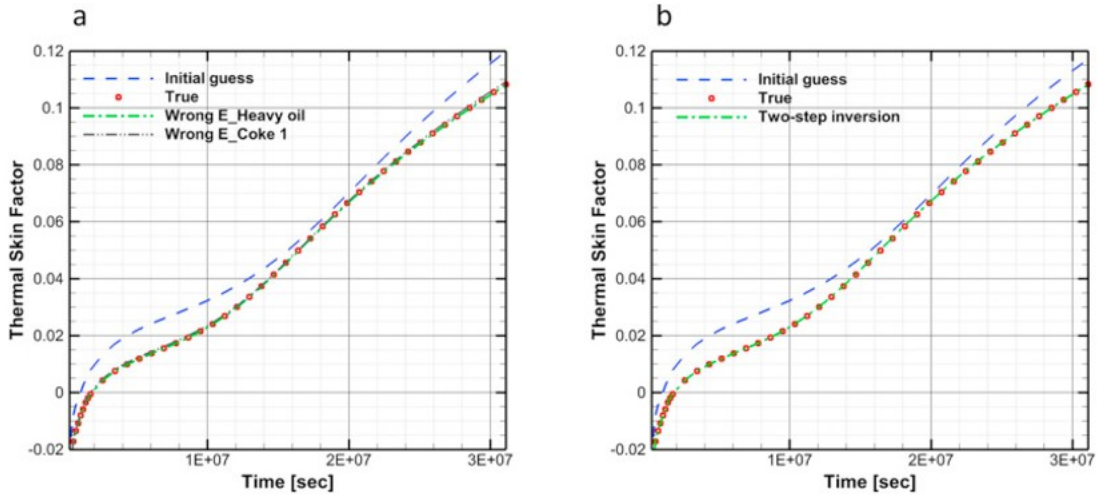

Fig. 7. Match of thermal skin factor as a function of time. (a) Case 4 (incorrect parameters), (b) case 5 (two-step inversion).

4.2.3. Performance of calibrated models

We evaluated the performance of the calibrated model in each case by comparing the spatial distributions of system conditions and properties, such as temperature, pressure, phases saturations, fractions of components in phases, relative permeability, capillary pressure, and phases properties like density, viscosity, and mobility.

Here, we provided the profiles of porosity and kerogen volume fraction in solid phase in the formation at t = 360 days, as they showed easily distinguishable differences between initial guess and calibrated model or true model, even though every profile showed great match between true models and calibrated models. In addition to this, porosity and kerogen volume fraction imply the information on the amount of solid components, which are composed with the reactant (= kerogen) and products (= cokes) as described in Eq. (3), as well as system conditions.

As can be seen in Fig. 8 and Fig. 9, it is found that the best calibrated model, which resulted minimum standard deviations of estimated parameters, well reproduced the spatial distributions of porosity and kerogen volume fraction in the system in every case of KR = 2.0, 2.25, and 2.5 $W\,(m\,K)^{-1}$.

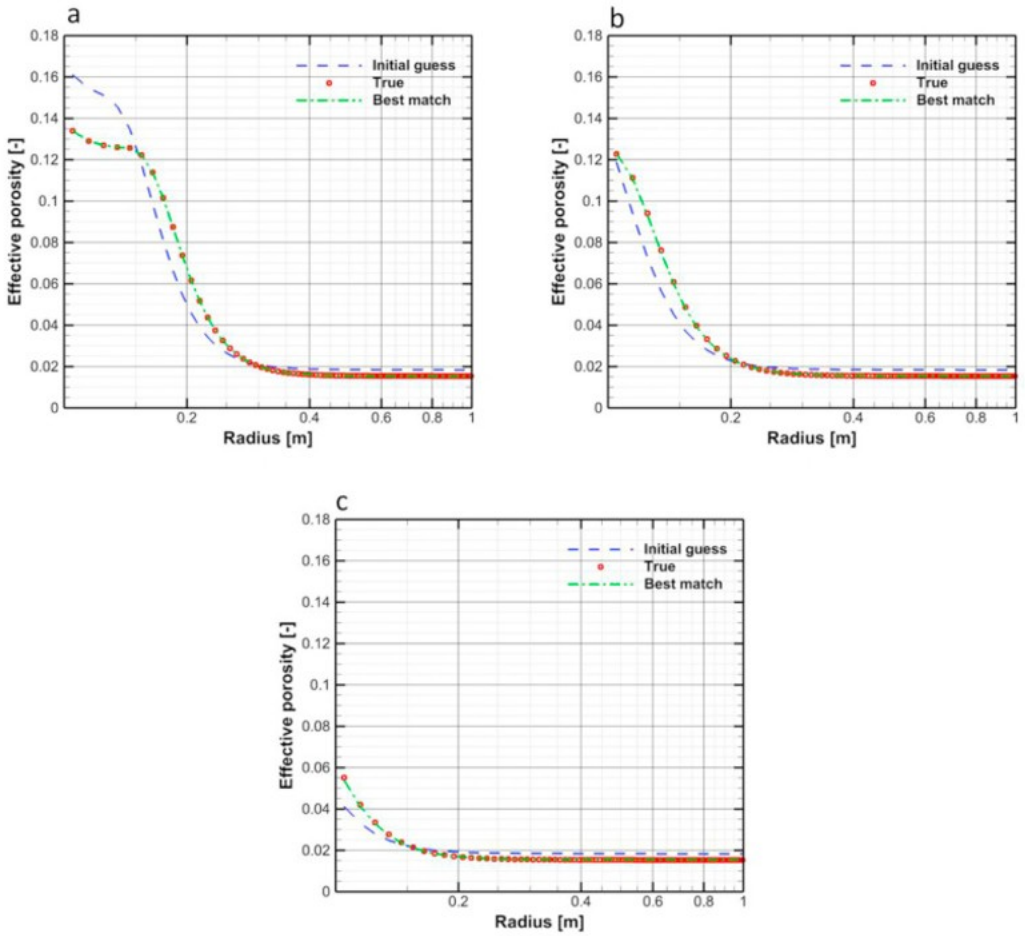

Fig. 8. Profiles of porosity distribution. (a) KR $= 2.0\,\mathrm{W\,(m\,K)^{-1}}$, (b) KR $= 2.25\,\mathrm{W\,(m\,K)^{-1}}$, (c) KR $= 2.5\,\mathrm{W\,(m\,K)^{-1}}$.

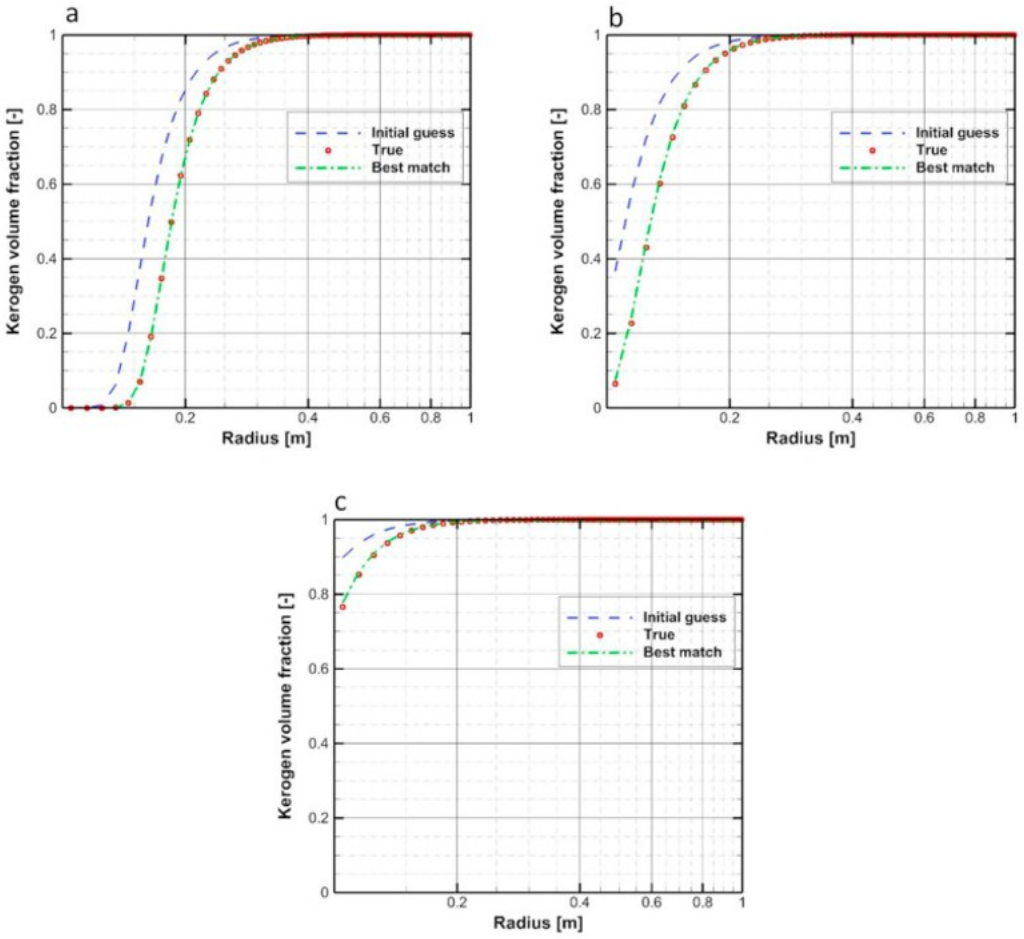

Fig. 9. Profiles of kerogen volume fraction distribution. (a) KR $= 2.0\,\mathrm{W\,(m\,K)^{-1}}$, (b) KR $= 2.25\,\mathrm{W\,(m\,K)^{-1}}$, (c) KR $= 2.5\,\mathrm{W\,(m\,K)^{-1}}$.

5. Conclusions

In this study, we proposed an inverse modeling approach that estimates unknown oil shale grade and activation energies of decomposition reactions of oil shale pyrolysis. The proposed approach suggested the inversion method incorporated with the concepts of temperature transient analysis and thermal skin effect. The proposed inversion method uses the observed heater temperature while heating the oil shale formation.

We have drawn following conclusions.

(1) From a sensitivity analysis of observation data—temperature difference and its derivative at the heater—to the unknown parameters, we found the most influential parameters on the observation data: Oil shale grade and activation energy of kerogen decomposition were the most influential parameters. The effects of activation energies of heavy oil and coke 1 decompositions on the observation data were only detectable in the late

time period of heating in the formation with dry rock thermal conductivity $= 2.0\,\mathrm{W\,(m\,K)^{-1}}$.

(2) We investigated the various cases of inverse modeling. The proposed inverse modeling method well estimates the unknown oil shale grade and activation energy of kerogen decomposition, regardless of thermal conductivity of dry rock. In overall, the proposed inversion approach showed an excellent performance by resulting the maximum relative errors of 3.93% and 1.43% for the estimation of oil shale grade and the activation energy of kerogen, respectively.

(3) We analyzed the activation energies of heavy oil and coke 1 decompositions in the case of formation with dry rock thermal conductivity $= 2.0\,\mathrm{W\,(m\,K)^{-1}}$. Firstly, we analyzed the impact of incorrectly assumed values for them. The incorrect activation energies made discrepancies in terms of thermal skin factor, between true model and calibrated model in late time period of heating. Secondly, we estimated them using two-step inversion approach. Here, oil shale grade and activation energy of kerogen decomposition were estimated in the first step by observing temperature difference; and the activation energies of heavy oil and coke 1 decompositions were estimated in the second step by observing the derivative of temperature difference. By matching the thermal skin factor as a function of time, we found that the two-step approach reproduced good match between true model and calibrated model.

(4) Performance of calibrated models was evaluated by comparing spatial distributions of porosity and kerogen volume fraction in the system, and the best calibrated model in each case of dry rock thermal conductivity showed highly well-matching results. This approach is expected to be useful to estimate the unknown oil shale grade and activation energy of kerogen decomposition, only by measuring heater temperature, without core sampling and subsequent surface experiments.

(5) Envisioned studies will include the investigation of the impact of heterogeneous reservoirs, to extend a range of application.

Acknowledgments

The authors appreciate Crisman Institute of Texas A&M University, since this work could be developed from its support. The authors also appreciate the funding sources of Lawrence Berkeley National Laboratory with the Office of Energy Efficiency and Renewable Energy and the Office of Fossil Energy of U.S. Department of Energy.

Nomenclature

Variables

A_j

frequency factor of decomposition reaction of j

Cκ
concentration of component
Cp
specific heat capacity
h
thickness of heating interval
hβ
specific enthalpy of phase β
F
mass flux
Ej
activation energy
J
Jacobian matrix
k
permeability
K
thermal conductivity
Kj
reaction rate constant
M
oil shale grade
qh
heat injection rate
rD
dimensionless radius
rj
reaction rate of decomposition reaction
rw
wellbore radius
s
stoichiometric coefficient

S
thermal skin factor
Sβ
saturation of phase β
Sij
sensitivity coefficient
S¯ij
scaled sensitivity coefficient
tD
dimensionless time
T
temperature
TD
dimensionless temperature
Vkerogen,i
initial volume fraction of kerogen
X
mass fraction
Δhj
reaction enthalpy
ΔT
temperature difference
ΔT'
derivative of temperature difference
μ
viscosity
ρ
density
σpj
parameter scaling factor
σzi
output scaling factor

φ

porosity

References

Bahrami and Siavoshi, 2007

H. Bahrami, J. Siavoshi**A new method in well test interpretation using temperature transient analysis for gas wells**

International Petroleum Technology Conference (2007)

(International Petroleum Technology Conference)

Berkovich et al., 2000

A.J. Berkovich, J.H. Levy, S.J. Schmidt, B.R. Young**Heat capacities and enthalpies for some Australian oil shales from non-isothermal modulated DSC**

Thermochim. acta, 357 (2000), pp. 41-45

Braun and Burnham, 1992

R.L. Braun, A.K. Burnham**PMOD: a flexible model of oil and gas generation, cracking, and expulsion**

Org. Geochem., 19 (1–3) (1992), pp. 161-172

Burnham and McConaghy, 2014

A.K. Burnham, J.R. McConaghy**Semi-open pyrolysis of oil shale from the garden gulch member of the Green river formation**

Energy & Fuels, 28 (12) (2014), pp. 7426-7439

Campbell et al., 1978

J.H. Campbell, G.H. Koskinas, N.D. Stout**Kinetics of oil generation from Colorado oil shale**

Fuel, 57 (6) (1978), pp. 372-376

Eseme et al., 2007

E. Eseme, J. Urai, B. Krooss, R. Littke**Review of mechanical properties of oil shales: implications for exploitation and basin modelling**

Oil Shale, 24 (2) (2007), pp. 159-175

Finsterle, 1999

S. Finsterle**iTOUGH2 User's Guide. LBNL-40040: 130**

(1999)

Finsterle and Zhang, 2011

S. Finsterle, Y. Zhang**Solving iTOUGH2 simulation and optimization problems using the PEST protocol**

Environ. Model. Softw., 26 (7) (2011), pp. 959-968

Fowler and Vinegar, 2009

T.D. Fowler, H.J. Vinegar**Oil shale ICP-Colorado field pilots**

SPE Western Regional Meeting, Society of Petroleum Engineers(2009)

Kar and Hascakir, 2017

T. Kar, B. Hascakir**In-situ kerogen extraction via combustion and pyrolysis**

J. Petroleum Sci. Eng. (2017)

Krauss and Mays, 2014

E.D. Krauss, D.C. Mays**Modification of the kozeny-carman equation to quantify formation damage by fines in clean, unconsolidated porous media**

SPE Reserv. Eval. Eng., 17 (04) (2014), pp. 466-472

Lee, 1982

J. Lee**Well Testing**

Society of Petroleum Engineers, New York (1982)

Lee et al., 2016

K.J. Lee, G.J. Moridis, C.A. Ehlig-Economides**A comprehensive simulation model of kerogen pyrolysis for the in-situ upgrading of oil shales**

SPE J. (2016)

Maes et al., 2016

J. Maes, A.H. Muggeridge, M.D. Jackson, M. Quintard, A.Lapene**Modelling in-situ upgrading of heavy oil using operator splitting method**

Comput. Geosci., 20 (3) (2016), pp. 581-594

Millington and Quirk, 1961

R. Millington, J. Quirk**Permeability of porous solids**

Trans. Faraday Soc., 57 (1961), pp. 1200-1207

Moridis et al., 2006

G. Moridis, M. Kowalsky, S. Finsterle, K. Pruess**TOUGH+: the new generation of object-oriented family of codes for the soluation of problems of flow and transport in the subsurface**

Proceedings of the TOUGH Symposium (2006)

Muradov and Davies, 2012

K. Muradov, D. Davies**Temperature transient analysis in horizontal wells: application workflow, problems and advantages**

J. Petroleum Sci. Eng., 92 (2012), pp. 11-23

Onur and Cinar, 2017

M. Onur, M. Cinar**Analysis of sandface-temperature-transient data for slightly compressible, single-phase reservoirs**

SPE J. (2017)

Phillips, 1991

O.M. Phillips**Flow and Reactions in Permeable Rocks**

Cambridge University Press (1991)

Pruess et al., 1999

K. Pruess, C. Oldenburg, G. Moridis**TOUGH2 User's Guide Version 2**

Lawrence Berkeley National Laboratory (1999)

Reynolds et al., 1991

J.G. Reynolds, R.W. Crawford, A.K. Burnham**Analysis of oil shale and petroleum source rock pyrolysis by triple quadrupole mass spectrometry: comparisons of gas evolution at the heating rate of 10 C/Min**

Energy Fuels., 5 (3) (1991), pp. 507-523

Smith, 1976

J. Smith**Relationship between Rock Density and Volume of Organic Matter in Oil shales.[Linear Equation Specific for Green River Formation Oil Shales], Energy Research and Development Administration**

Laramie Energy Research Center, Laramie, Wyo. (USA) (1976)

Stehfest, 1970

H. Stehfest**Algorithm 368: numerical inversion of Laplace transforms [D5]**

Commun. ACM, 13 (1) (1970), pp. 47-49

Steingrímsson, 2013

B. Steingrímsson**Geothermal Well Logging: Temperature and Pressure Logs. Tutorial-geothermal Training Programme**

(2013)

Sui et al., 2012

W. Sui, C. Ehlig-Economides, D. Zhu, A. Hill**Determining multilayer formation properties from transient temperature and pressure measurements**

Petroleum Sci. Technol., 30 (7) (2012), pp. 672-684

Vinegar, 2006

H. Vinegar

Shell's In-situ Conversion Process, 26th Oil Shale Symposium, Golden, Colorado, October 16, Pp. 2006 (2006)

Wen and Kobylinski, 1983

C.S. Wen, T.P. Kobylinski**Low-temperature oil shale conversion**

Fuel, 62 (11) (1983), pp. 1269-1273

Woods, 1999

A.W. Woods**Liquid and vapor flow in superheated rock**

Annu. Rev. fluid Mech., 31 (1) (1999), pp. 171-199

Youtsos et al., 2013

M. Youtsos, E. Mastorakos, R. Cant**Numerical simulation of thermal and reaction fronts for oil shale upgrading**

Chem. Eng. Sci., 94 (2013), pp. 200-213